Journal Pre-proof

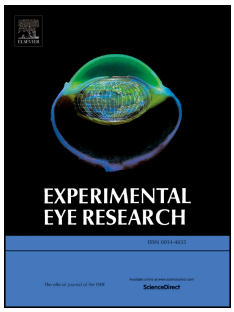

Extracellular Vesicle–Mediated Delivery of miR-181a-3p Confers Neuroprotection to Degenerating Retinal Ganglion Cells

Esmahan Durmaz, Kubra Trabzonlu, Maryam Esmaeili, Hanady Nehme, Lydia Alverez-Erviti, Yasir Ahmed Syed, Aled Clayton, Ben Mead

PII: S0014-4835(26)00038-2

DOI: https://doi.org/10.1016/j.exer.2026.110882

Reference: YEXER 110882

To appear in: *Experimental Eye Research*

Received Date: 6 October 2025

Revised Date: 18 December 2025

Accepted Date: 21 January 2026

Please cite this article as: Durmaz, E., Trabzonlu, K., Esmaeili, M., Nehme, H., Alverez-Erviti, L., Syed, Y.A., Clayton, A., Mead, B., Extracellular Vesicle–Mediated Delivery of miR-181a-3p Confers Neuroprotection to Degenerating Retinal Ganglion Cells, *Experimental Eye Research*, https://doi.org/10.1016/j.exer.2026.110882.

Extracellular Vesicle–Mediated Delivery of miR-181a-3p Confers Neuroprotection to Degenerating Retinal Ganglion Cells

Esmahan Durmaz[1,2], Kubra Trabzonlu[3,4], Maryam Esmaeili[1], Hanady Nehme[1], Lydia Alverez-Erviti[5], Yasir Ahmed Syed[3,4], Aled Clayton[6], Ben Mead[1*]

1. School of Optometry and Vision Sciences, Cardiff University, Cardiff, UK
2. Department of Genetic and Bioengineering, Alanya Alaaddin Keykubat University, Antalya, Türkiye
3. Neuroscience and Mental Health Innovation Institute, Hadyn Ellis Building, Cardiff University, Cardiff, UK
4. School of Bioscience, Cardiff University, Cardiff, UK
5. Laboratory of Molecular Neurobiology, Centre for Biomedical Research of La Rioja, Logroño, Spain
6. School of Medicine, Cardiff University, Cardiff, UK

*Corresponding author at - School of Optometry and Vision Sciences, Cardiff University, Cardiff, UK, CF24 4HQ. MeadB@Cardiff.ac.uk

Abbreviations:

EV: Extracellular vesicles

RGC: Retinal ganglion cell

IOP: Intraocular pressure

MSC: Mesenchymal Stem Cell

Tuj 1: Class III β-Tubulin

Brn3a: Brain specific homeobox/POU domain protein 3A

DPBS: Dulbecco's Phosphate Buffered Saline

CNTF: Ciliary Neurotrophic factor

PPD: Paraphenylenediamine

PFA: Paraformaldehyde

ONC: Optic Nerve Crush

IPA: Ingenuity Pathway Analysis

ESC: Embryonic stem cell

SD rats: Sprague Dawley rats

CNS: Central nervous system

SEMA3A: Semaphorin 3A

P38/ERK/JNK: p38/extracellular signal-regulated kinase/c-Jun N-terminal kinase

TNF-α: Tumor necrosis factor-alpha

KCl: Potassium Chloride

NaCl: Sodium Chloride

NaHCo3: Sodium Bicarbonate

KH2PO4: Monopotassium phosphate

MgCl2: Magnesium chloride

CaCl2: calcium chloride

FGF: Fibroblast growth factor

PDGF: Platelet derived growth factor

p38/MAPK: p38 mitogen-activated protein kinase

AU (ATU): arbitrary unit

GAPDH: Glyceraldehyde 3-phosphate dehydrogenase

BMSC: Bone marrow stem cell

Abstract

Background:
Glaucoma is a progressive optic neuropathy marked by the irreversible degeneration of retinal ganglion cells (RGCs), leading to vision loss. RGC injury is also central to other optic and neurodegenerative conditions, including traumatic optic neuropathy.

Purpose:
We evaluated whether extracellular vesicles (EVs) derived from retinal precursor cells could serve as an effective platform for the delivery of neuroprotective microRNAs (miRNAs), focusing on miR-181a-3p, to preserve RGC viability and function.

Methods:
Based on prior profiling of miRNAs differentially expressed in injured RGCs, four candidate miRNAs were screened for neuroprotective effects in primary rat retinal cultures and human embryonic stem cell–derived RGCs. miR-181a-3p, which showed the strongest preservation of RGC survival, was selected for further study. EVs were isolated from R-28 retinal precursor cells, loaded with miR-181a-3p via electroporation, and characterized for particle size, charge, and loading efficiency. EV uptake and neuroprotective efficacy were evaluated *in vitro* by fluorescence imaging, qPCR, and Ca^{2+}-activity assays, and *in vivo* by intravitreal injection of labelled EVs to assess retinal distribution and cellular uptake.

Results:
EV-mediated delivery of miR-181a-3p enhanced RGC survival and preserved intracellular Ca^{2+} dynamics compared to free miRNA or lipofectamine-based transfection. EVs improved miRNA stability, enabled selective targeting of retinal cell types, and partially modulated the p38/MAPK signalling axis. EV loading also improved the delivery of miRNA to the retina *in vivo.*

Conclusion:
Our findings demonstrate that EVs offer a biocompatible, cell-specific, and functionally effective platform for miRNA delivery to the retina. EV-based administration of miR-181a-3p may represent a novel neuroprotective strategy for glaucoma and related optic neuropathies.

Funding: The authors acknowledge the following sources of financial support. Esmahan Durmaz and Kubra Trabzonlu were supported by a Ph.D. scholarship from the YLSY program of the Republic of Turkiye, Ministry of National Education. This project was funded by Cardiff University Hodge ECR funding and Cardiff University School of Optometry and Vision Sciences EGAS grant. This work was also funded by Fight for Sight UK, grant reference # 5183/5184.

Introduction

Glaucoma is a neurodegenerative disease characterized by progressive retinal ganglion cell (RGC) apoptosis, ultimately leading to irreversible vision loss. This multifactorial condition involves interconnected mechanisms including neurotrophic factor deprivation, hypoxia, glutamate excitotoxicity, and inflammation. Current experimental therapies target these degenerative pathways, but no clinically approved neuroprotective interventions exist for glaucoma to date.

MicroRNAs (miRNAs) are small, non-coding RNAs that downregulate mRNA translation and regulate post-transcriptional gene expression. Their capacity to modulate multiple signalling pathways makes them promising candidates for neuroprotective therapy. For instance, miR-149 downregulation alters betacellulin expression and attenuates RGC apoptosis (Nie et al., 2018), while miR-30b promotes axon regeneration via inhibition of SEMA3A (Chan-Juan et al., 2019). Similarly, miR-200a has been shown to confer neuroprotection by inhibiting fibroblast growth factor expression and components of the p38/ERK/JNK pathway (Peng et al., 2019).

Our previous investigations evaluated six miRNAs delivered in triplicate cocktails via viral vectors in an *in vivo* model of optic nerve crush. A combination of miR-17-5p, miR-30c-2, and miR-92a, as well as a second cocktail of miR-92a, miR-292, and miR-182, demonstrated significant RGC neuroprotection and preservation of retinal function (Mead et al., 2020). Further, miR-124 delivery has been shown to preserve RGCs through mechanisms involving autophagic regulation via the P2X7-Akt/mTOR axis (Chen et al., 2023; Guo et al., 2022). Notably, miR-124 also supports axon growth in RGCs derived from Müller glia (He et al., 2018) and contributes to intraocular pressure (IOP) regulation (Li et al., 2020).

Extracellular vesicles (EVs), lipid bilayer-enclosed nanoparticles secreted by virtually all cell types, serve as natural carriers of proteins, lipids, and nucleic acids. Their biocompatibility, low immunogenicity, and ability to cross biological barriers position them as ideal drug delivery vectors. Our earlier work demonstrated that EVs derived from bone marrow mesenchymal stem cells (MSCs) mediate RGC neuroprotection via endogenous miRNA cargo (Mead & Tomarev, 2017). Subsequent studies have validated the efficacy of EV-based therapies in RGC degeneration models (Mead &

Tomarev, 2020), and our recent work confirms the neuroprotective potential of R-28 retinal precursor cell-derived EVs (Durmaz et al., 2025).
Given their ability to deliver therapeutic cargo, many studies have investigated EVs as a drug delivery system for candidate therapeutics loaded into them, such as miRNAs and proteins (Alvarez-Erviti et al., 2011; Ilahibaks et al., 2023; Izco et al., 2023; Yang et al., 2017)).

EVs can be engineered for therapeutic delivery (Durmaz et al., 2024) through **pre-loading**, modifying the donor cells during EV biogenesis, or **post-loading**, in which isolated EVs are directly loaded with therapeutic agents. For example, TNF-α pre-conditioning of MSCs yields EVs with enhanced therapeutic potency (Mead et al., 2020), while post-loaded nicotinamide EVs have demonstrated superior efficacy in preserving RGC arborization compared to unloaded controls (Kim et al., 2024).

We hypothesized that EVs derived from the R-28 cell line could serve as an effective platform for miRNA delivery to the retina. This study aimed to develop a non-cell-based method to achieve targeted miRNA delivery for RGC neuroprotection. Building on our prior miRNA profiling of healthy and injured RGCs (Mead et al., 2021), we screened multiple candidates, including miR-16a-5p inhibitor, miR-23a-3p inhibitor, miR-181a-5p mimic, and miR-194-5p inhibitor, and identified miR-181a-3p as a lead neuroprotective molecule. We assessed its delivery via R-28 EVs *in vitro* and *in vivo*, and found that EV-mediated delivery significantly improved the delivery efficacy of therapeutic RNA to the retina and in particular, the RGC.

Methods

All experiments were done at n=3 with the experimental unit defined as: A), a single retinal culture from a single rat; B), an RGC culture from an independent embryonic stem cells (ESC) differentiation; and C), an individual rat. For A and B, three technical repeats (separate culture wells) were included per biological repeat. All analysis was done with the investigator blind to the treatment groups.

R-28 Cell Culture

R-28 cells, generously provided by Dr. Gail Seigel (Seigel, 2014) and previously validated by short tandem repeat analysis, were cultured in Dulbecco's Modified Eagle Medium (Gibco, MA, USA) supplemented with 10% exosome-depleted fetal bovine serum (Sigma, MO, USA) and 1% penicillin-streptomycin (Gibco). Cells were maintained at 37 °C with 5% CO_2 and harvested at 80–90% confluency. Conditioned media were collected and stored at –80 °C for subsequent EV isolation.

EV Isolation and Characterization

EVs were isolated from R-28 cell culture supernatants by differential ultracentrifugation. Conditioned media were first centrifuged at 300 × g for 10 minutes to remove cells, followed by 2,000 × g for 20 minutes to eliminate debris and apoptotic bodies. The supernatant was then filtered (0.22 µm) and ultracentrifuged at 100,000 × g for 90 minutes (Beckman Coulter Optima). The resulting EV pellet was resuspended in PBS and stored at –80 °C.

Following miRNA loading via electroporation, EVs were washed by repeat ultracentrifugation (100,000 × g, 70 minutes) to remove unincorporated miRNA and residual electroporation buffer, which could introduce salt crystals and interfere with downstream quantification. EV size, concentration, and surface charge (zeta potential) were then assessed using the PMX-230-Z-Twin ZetaView Nanoparticle Tracking Analyzer (Particle Metrix, Germany) at 25 °C and confirmed enriched for CD9, CD63, and CD81 using a ZetaView compatible tetraspanin detection kit (#700381, Particle Metrix). Briefly, antibodies are incubated with $1x10^{10}$ EVs for 1 hour in the dark, before quantification using the ZetaView (excitation 490nm/emission 516nm). IgG antibody is used as a negative control.

Primary Rat Retinal Ganglion Cell (RGC) Culture

Primary RGCs were prepared from adult Sprague Dawley rats (~200 g) as previously described (Durmaz et al., 2023). Following CO_2 euthanasia and enucleation, retinas were enzymatically dissociated using papain and DNase I (Worthington Biochemical, NJ, USA) for 90 minutes at 37 °C. After centrifugation (300 × g, 5 min), cells were washed and layered onto a discontinuous albumin-ovomucoid inhibitor density gradient and centrifuged (70 × g, 6 min). The pellet was resuspended and plated at 125,000 cells/well in 8-well chamber slides pre-coated with poly-D-lysine and laminin

(Sigma). Cells were cultured in Neurobasal-A medium with B27 and L-glutamine (Gibco).

Transfection & Treatments

Candidate miRNAs (Table 1) were prepared using a commercial transfection reagent (Lipofectamine), following the manufacturer's protocol. Treatment groups included: 1), Vehicle control (transfection reagent only); 2), Free miRNA (50nM); 3), miRNA-loaded EVs (50nM of miRNA); and 4), ciliary neurotrophic factor (CNTF; 50 nM; positive control). Cells were incubated for 3 days before immunocytochemistry.

	miRbase Accession Number	Mature miRNA Sequence
miR-16a-5p inhibitor	MIMAT0000785	UAGCAGCACGUAAAUAUUGGCG
miR-23a-3p inhibitor	MIMAT0000792	AUCACAUUGCCAGGGAUUUCC
miR-181a-5p mimic	MIMAT0014641	ACCAUCGACCGUUGAUUGUACC
miR-194-5p inhibitor	MIMAT0000869	UGUAACAGCAACUCCAUGUGGA

Table 1. *The list of candidate miRNA used in this study along accession numbers and sequences. Note that for 3 of the candidates, inhibitors were used.*

Immunocytochemistry

Cells were fixed with 4% paraformaldehyde (10 min), washed in PBS (3 × 10 min), and blocked with 3% BSA/0.1% Triton X-100 for 20 minutes. They were incubated with mouse anti-βIII-tubulin (1:500, Sigma) for 1 hour, followed by Alexa Fluor 488-conjugated goat anti-mouse IgG (1:400, ThermoFisher, A32723) for 1 hour. Nuclei were stained with DAPI (Vectashield), and imaging was performed using a Leica AF6000 system with LAS X software (v3.0.4.16529). We refer to RGC as large spherical βIII-tubulin$^+$ rat retinal cells which can be identified by preferential βIII-tubulin staining intensity around the axonal base. Approximately 60% of the retinal cells in this culture are neurons (neurofilament+/βIII-tubulin+), of which 10% are Thy1$^+$ RGCs and possess the unique βIII-tubulin staining pattern described above (Suggate et al., 2009). RGC were quantified in the entire well.

Quantitative PCR (qPCR)

RNA was extracted from RGCs (250,000 cells/well, 24 h post-treatment) using the RNeasy Mini Kit (Qiagen). cDNA was synthesized (appSCRIPT kit, Appleton Woods), followed by qPCR (qPCRBIO SyGreen Blue Mix Lo-ROX) using the StepOnePlus Real-Time PCR

System. Relative gene expression was calculated using the $2^{-}\Delta\Delta Ct$ normalization method with GAPDH as the reference gene. Primer sequences are listed in Table 2.

Primer name	Sequence
Caspase 3 Forward	GAGCTTGGAACGCGAAGAAA
Caspase 3 Reverse	TAACCGGGTGCGGTAGAGTA
Bcl2L1 Forward	CGCCGGAGATAGATTTGAATAACC
Bcl2L1 Reverse	TGCCAGGAGACCAAAAAGGG
p38 MAPK 14 Forward	TCGGCACACTGATGACGAAA
p38 MAPK 14 Reverse	TCATGGCTTGGCATCCTGTT
FGF7 Forward	TGGGCACTATATCTCTAGCTTGC
FGF7 Reverse	GGGTGCGACAGAACAGTCT
PDGF Forward	ACACCTGGATACCTCTCCCC
PDGF Reverse	CTGGCCTGGTCCTTCAATGG
miRNA 181a-3p Forward	ACCATGACCGTTGATTGTACC
miRNA 181a-3p Reverse	TGGTACTGGCAACTAACATGG

Table 2. *The list of primers used in qPCR quantification of mRNAs.*

miRNA Loading and Detection

EVs were isolated and electroporated with miR-181a-3p (550nmol, 700nmol, or 850nmol) using the Gene Pulser Xcell (Bio-Rad) at 400 V, 125 µF in 0.4 cm cuvettes. The electroporation buffer contained 1.15 mM potassium phosphate (pH 7.2), 25 mM KCl, and 21% Optiprep (Sigma). Post-electroporation, EVs were centrifuged at 100,000 × g to remove unincorporated miRNA. To quantify miRNA loading and cellular uptake, qPCR was performed on EV samples and on R-28 cells (2×10^4) transfected with miRNA-loaded EVs. EVs were then appropriately diluted to create EV prep that contained 50nM of the loaded miRNA.

miRNA Testing in Human RGCs

Human ESC-derived RGCs were generated via a 40-day small molecule differentiation protocol (Esmaeili & Mead, 2023; Sluch et al., 2017). Cells (125,000/well) were plated in 8-well chamber slides coated with 0.09mg/mL Growth factor reduced Matrigel (REF 356234, Corning) and treated with 1 µM colchicine to induce RGC degeneration alongside 50 nM CNTF or 50 nM miRNA. After 48 h, cells were fixed and nine images/well were acquired and analyzed

using ImageJ, quantifying RGC by their endogenous TdTomato fluorescence expressed under the RGC specific promoter brn3b.

Single-Cell Calcium Imaging

Primary RGCs (250,000/well) were treated with 50 nM miRNAs for 24 h. Cells were incubated with Cal-520 (1 μM; AAT Bioquest) in 0.02% Pluronic acid for 1 h. Imaging solution: 125 mM NaCl, 26 mM $NaHCO_3$, 1.25 mM KH_2PO_4, 2.5 mM KCl, 1 mM $MgCl_2$, 2 mM $CaCl_2$, 25 mM glucose. Time-lapse images (200 ms intervals, 5 min) were captured via epifluorescence microscopy and analyzed in MATLAB using NeuroCa.

EV Labeling and Tracking

To track RNA delivery, EVs were labeled with siGlo (Horizon Discovery, 100 nM) or Alexa Fluor 647 C2 maleimide (ThermoFisher). For dye purification, MW3000 spin columns (ThermoFisher) were used per manufacturer's protocol. EV uptake was assessed in R-28 cells or fibroblasts at 30, 60, and 180 minutes. After 24 h, cells were fixed, permeabilized (methanol, 15 min), and counterstained with DAPI. Confocal images were analyzed using ImageJ. To assess cell specificity and delivery efficiency, comparisons were made between: 1), R-28-derived EVs on R-28 cells or fibroblasts; 2), Fibroblast-derived EVs on R-28 cells and 3), naked RNA and unloaded EV controls on R-28 cells or fibroblasts.

***In vivo* delivery of siGlo-loaded EVs.**

All experiments were performed under the United Kingdom Animals (Scientific Procedures) Act 1986 after approval from the Home Office and local AWERB committee. Adult Sprague Dawley rats (150-200g) were injected with $3x10^9$ EVs loaded with an optimal 700nmol siGlo RNA. Animals were euthanised by rising concentration of CO_2 at both 1- and 24-hours post-injection. Vitreous and retina were collected. Retina was digested as above, with RGC purified by incubating with CD90.1 magnetic beads as per the manufacturer's instructions (#130-096-209; Miltenyi Biotec, Auburn, CA, USA). Briefly, retinal cells were incubated with CD90.1

enrichment and CD11b depletion antibodies conjugated to magnetic beads. Following depletion, the retinal suspension is passed through a magnetized column and the enriched RGC are collected. Vitreous samples, retinal cell fractions depleted of RGCs, and purified RGCs were assayed for SiGlo fluorescence using an OmegaStar microplate reader (BMG Labtech, Ortenberg, Germany),

Statistics

All statistical tests were performed using SPSS 17.0 (IBM SPSS, Inc., Chicago, IL, USA) and data presented as mean +/- SEM with graphs constructed using Graphpad Prism 7.01 (Graphpad Prism, La Jolla, CA, USA). The Shapiro-Wilkes test was used to ensure all data were normally distributed before parametric testing using a 1-way ANOVA with a Tukey post hoc test. Statistical differences were considered significant at P values < 0.05.

Results

In Vitro Evaluation of Candidate miRNAs in Rodent and Human Retinal Ganglion Cells

To identify neuroprotective microRNAs, we selected four candidates based on their differential abundance in glaucomatous vs. healthy RGCs previously reported in our miRNA profiling study (Mead et al., 2021): miR-16a-5p, miR-23a-3p, miR-181a-3p, and miR-194-5p. These were tested as inhibitors (for miR-16a-5p, miR-23a-3p, and miR-194-5p) or mimics (for miR-181a-3p) in primary rodent retinal cultures (**Fig. 1**). RGCs were defined morphologically and immunocytochemically as βIII-tubulin$^+$ neurons with localized soma staining. Due to known cytotoxicity of cationic transfection reagents in neurons, lipofectamine-only treated wells served as the negative control. Day 1 post-treatment, RGC survival was highest in wells treated with miR-181a-3p mimic (717 ± 167.4 cells/well) and miR-194-5p inhibitor (943 ± 302.3 cells/well), compared to lipofectamine control (309 ± 111.8 cells/well; p = 0.099), trending toward neuroprotection, but falling short of statistical significance until the later time points. Day 2, overall RGC survival declined in all groups. However, the miR-181a-3p mimic continued to show robust neuroprotection (21.4% RGC loss vs. 57.0% in control). miR-194-5p also preserved significantly more RGCs than controls (224 ± 130.4 vs. 101.7 ± 46.7 cells/well). By Day 3, the protective effect of miR-181a-3p mimic persisted (195.3 ± 76.1 cells/well), along with miR-23a-3p inhibitor (214.3 ± 39.4), compared to the control group (83.0 ± 44.0; p < 0.05 for both comparisons).

These results collectively suggest that **miR-181a-3p mimic** and **miR-194-5p inhibitor** confer sustained neuroprotection to RGCs *in vitro*, even under conditions of progressive degeneration.

The neuroprotective capacity of miR-181a-3p and miR-23a-3p were validated in a human embryonic stem cell-derived RGC model subjected to colchicine-induced injury. Consistent with rodent data, miR-181a-3p trended towards enhanced human RGC survival (989.7 ± 504.9 cells/well, $n = 3$), compared to lipofectamine-only controls (372.7 ± 69.5 cells/well, $n = 3$; **Fig. 1**). These findings indicate that miR-181a-3p may confer cross-species neuroprotection to RGCs and is a strong candidate for further therapeutic evaluation.

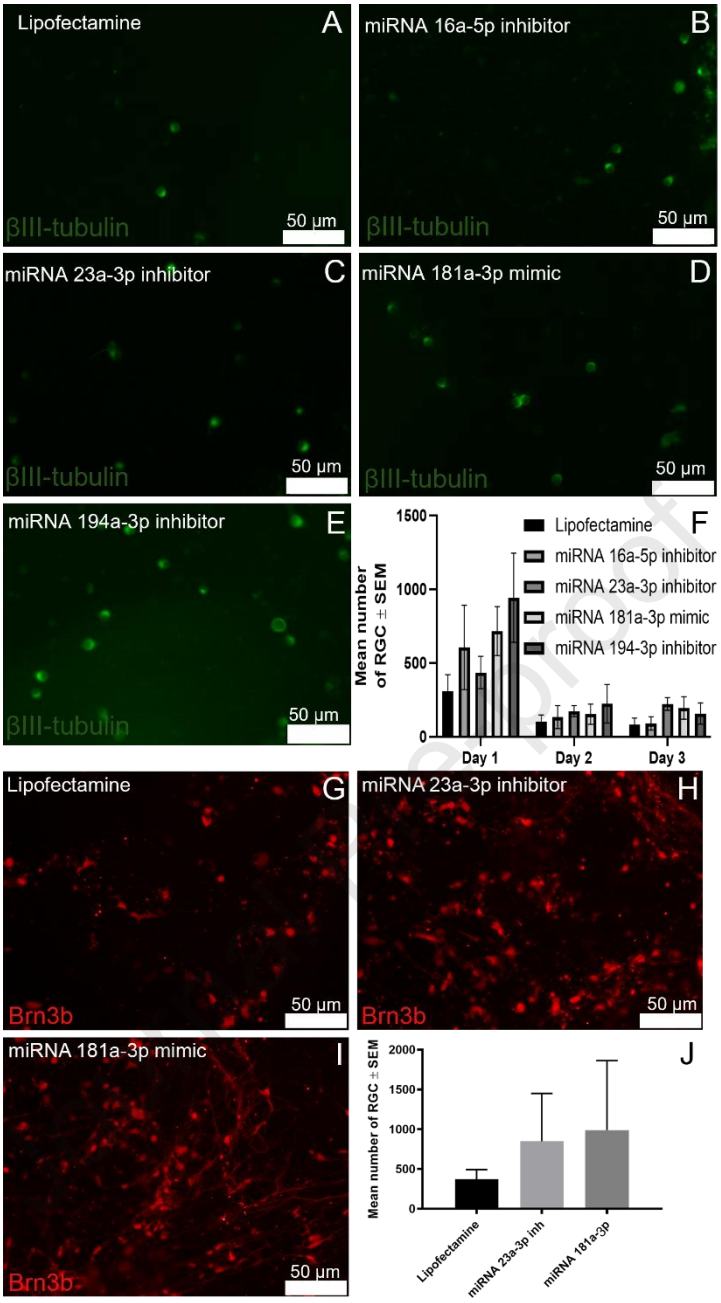

Figure 1. Neuroprotective effects of candidate miRNAs on rat and human retinal ganglion cells. Primary rat retinal cultures were treated with lipofectamine (control; A), miR 16a-5p inhibitor (B), miR 23a-3p inhibitor (C), miR 181a-3p mimic (D), and miR 194-5p inhibitor (E). Graph shows the mean number of surviving RGCs (βIII-tubulin^{+}; green) across three time points per well (F). Human retinal ganglion cell cultures were treated with lipofectamine (control; G), miR 23a-3p (H), and miR 181a3p (I). Graph shows the mean number of surviving RGC per region of interest (J). All data are presented as mean ± SEM (n = 3).

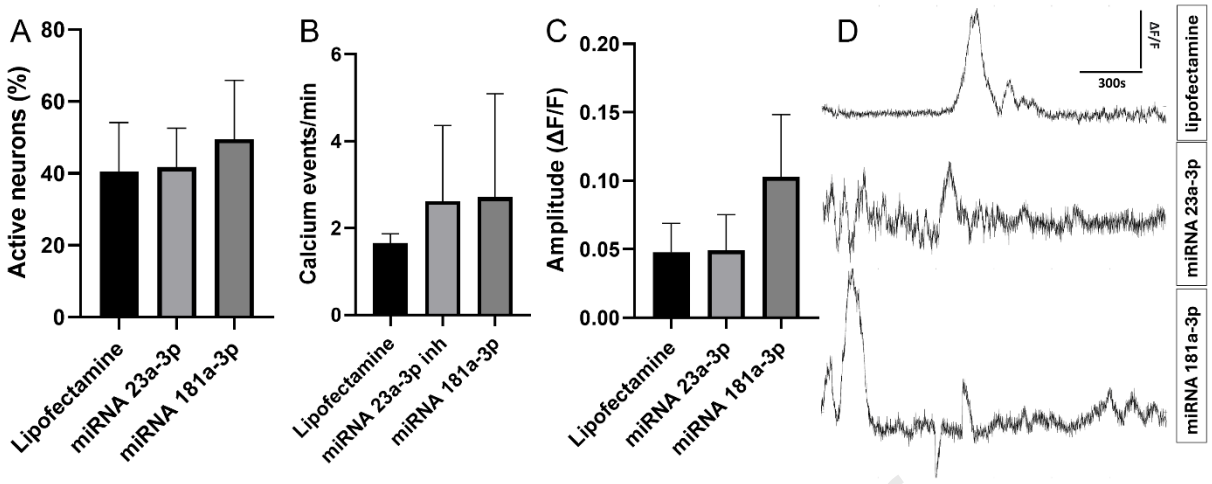

Figure 2. Calcium transient activity in RGCs following miRNA treatment. Primary RGCs were treated with lipofectamine (control), miR-23a-3p inhibitor, or miR-181a-3p mimic. (A) Bar graph showing the percentage of active RGCs exhibiting at least one spontaneous calcium transient over a 5-minute period. (B) Graph showing the number of calcium events per minute per active RGC. (C) Graph showing the amplitude of calcium transients in responsive cells. Data are presented as mean ± SEM (n = 5), representative calcium transients are shown in D.

Preservation of Neuronal Activity in miRNA-Treated Retinal Ganglion Cells

To assess the functional integrity of RGCs following miRNA treatment, calcium imaging was performed on primary rat retinal cultures. RGC activity was evaluated based on three parameters: (1) the proportion of cells exhibiting at least one spontaneous calcium event over a 5-minute period (**Fig. 2A**), (2) the frequency of calcium transients (**Fig. 2B**), and (3) cytosolic calcium amplitude dynamics (**Fig. 2C**).

Treatment with miR-181a-3p mimic resulted in a trend toward enhanced preservation of RGC functionality, with approximately 50% of cells displaying spontaneous activity, compared to 40.4% in miR-23a-3p inhibitor treated wells and 41.7% in lipofectamine-only controls (p = 0.129; **Fig. 2A**).

Both miRNA treatments were associated with a modest increase in the number of calcium transients per cell (**Fig. 2B**), indicating a possible improvement in neuronal excitability. In particular, miR-181a-3p treatment also led to a trend toward elevated calcium transient amplitude compared to controls (p = 0.062; **Fig. 2C**), suggesting partial preservation of intracellular calcium signalling dynamics.

While these differences did not reach statistical significance, the consistent trends across multiple measures support the hypothesis that miR-181a-3p may help preserve RGC excitability and synaptic function under stress conditions.

Predicted Molecular Mechanisms Underlying miR-181a-3p Neuroprotection

To elucidate the potential mechanisms driving the neuroprotective effects of miR-181a-3p, we performed an *in silico* analysis using Ingenuity Pathway Analysis (IPA). Predicted mRNA targets of miR-181a-3p were mapped onto canonical pathways and functional networks relevant to RGC degeneration.

IPA revealed that miR-181a-3p is predicted to regulate components of the p38 MAPK signalling cascade, along with several neurotrophic and mitogenic growth factors, including fibroblast growth factor (FGF), epidermal growth factor (EGF), and platelet-derived growth factor (PDGF). Further filtering for apoptosis-related targets identified four candidate genes implicated in cell death signalling, one of which intersected with the p38 MAPK pathway. Enrichment analysis also highlighted biological processes related to metabolism, cellular regulation, and stress response, suggesting a multifaceted neuroprotective role.

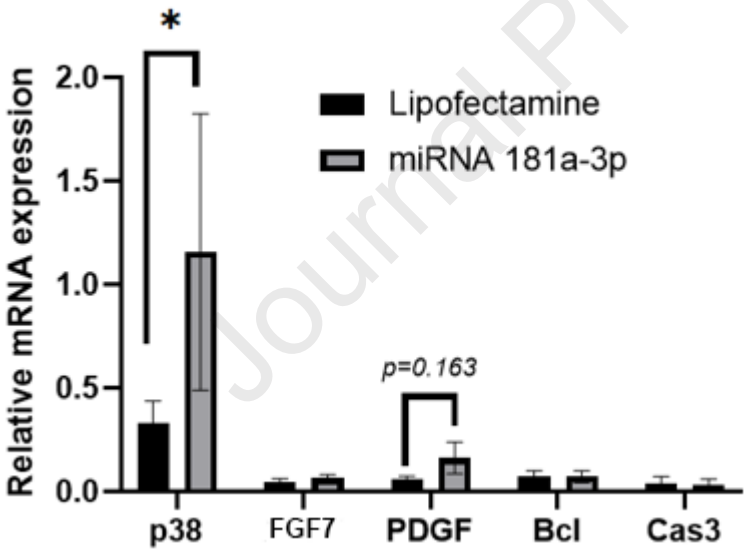

Figure 3. Expression of target genes following miR-181a-3p mimic treatment in primary retinal cells. qPCR analysis of p38 MAPK, FGF7, PDGF, Bcl-2, and Caspase-3 mRNA expression after 24 hours of treatment. Data are shown as mean ± SEM (n = 6–8).

To experimentally validate the pathway predictions, we treated primary rat retinal cultures with miR-181a-3p mimic for 24 hours and assessed target gene expression by qPCR. Among the candidate targets, p38 MAPK (p38) showed a trend toward upregulation in treated cells compared to controls (0.35 ± 0.15 vs. 0.11 ± 0.02; $p = 0.079$; **Fig. 3**), whereas no significant differences were detected for FGF7, PDGF, Bcl, and Cas3.

These findings suggest that miR-181a-3p may exert neuroprotection in RGCs through partial modulation of the p38 MAPK pathway.

Efficient Loading and Delivery of miR-181a-3p via Electroporated Extracellular Vesicles

Given the cytotoxicity and poor *in vivo* compatibility of commercial transfection reagents, we evaluated electroporation as a strategy to load miR-181a-3p into EVs for delivery to retinal cells.

As a proof-of-concept, R-28-derived EVs were first loaded with a fluorescent siRNA reporter (siGlo). Following 24-hour incubation with R-28 cells, siGlo fluorescence intensity was significantly higher when delivered via R-28-derived EVs (242.3 ± 34.8 arbitrary units [AU]) compared to lipofectamine-mediated delivery (103.4 ± 23.8 AU; $p = 0.03$) or siRNA alone ($p = 0.004$) (**Fig. 4A, B**). Notably, transfection efficiency was significantly reduced when fibroblast-derived EVs were used to deliver siRNA to R-28 cells (105.3 ± 23.5 AU; $p = 0.03$), or when R-28 EVs were used to deliver cargo into fibroblasts (142.7 ± 53.4 AU), indicating cell-type specificity in EV-mediated delivery.

We next assessed the optimal loading conditions for miR-181a-3p. Varying concentrations of miRNA were electroporated into a fixed number of R-28 EVs (~3×10^9 particles). Quantification by qPCR showed that 700 nmol of miRNA yielded the highest loading efficiency ($p = 0.039$; **Fig. 4C**).

To determine functional delivery, R-28 cells were treated with miR-181a-3p-loaded EVs, and intracellular miRNA levels were measured after 24 hours. EV-mediated delivery resulted in higher intracellular levels of miR-181a-3p compared to lipofectamine-treated or untreated cells ($p = 0.065$; **Fig. 4D**).

Together, these results demonstrate that electroporated EVs outperform commercial transfection reagents in both cargo loading and delivery to RGC-like cells, while offering cell-type specificity and potential for *in vivo* translation.

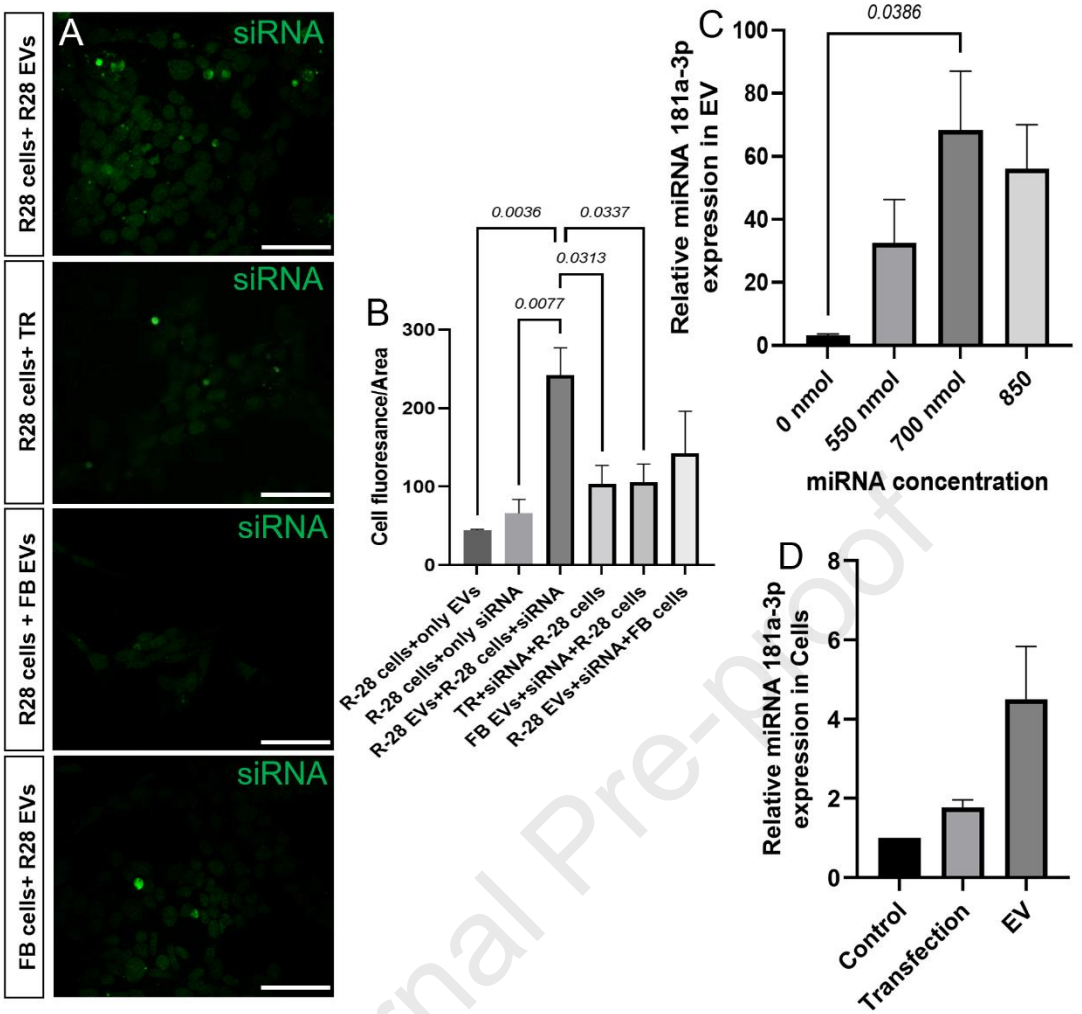

Figure 4. Efficient loading and cellular delivery of miRNAs via R-28-derived EVs. (A, B) Quantification of siGLO fluorescence intensity in R-28 cells following delivery via R-28 EVs, fibroblast EVs, transfection reagent, or naked siRNA. (C) Relative miR-181a-3p levels in EVs (normalized to GAPDH) at different input quantities post-electroporation. (D) Transfection efficiency assessed by intracellular miRNA levels in R-28 cells 24 hours after treatment with miR-181a-3p-loaded EVs or lipofectamine. Representative images show EV-mediated delivery of fluorescently labelled siRNA (green). Scale bar = 40× magnification; n = 3 per condition.

Electroporation-Induced Changes in EV Properties and Cell Targeting

To evaluate whether electroporation altered key properties of R-28-derived EVs, we compared particle number, size, and zeta potential before and after miRNA loading.

Particle concentration was slightly reduced following electroporation ($2.97 \times 10^9 \pm 1.0 \times 10^9$ EVs) compared to pre-electroporation levels ($4.20 \times 10^9 \pm 3.67 \times 10^8$ EVs), although the difference was not statistically significant ($p = 0.390$; **Fig. 5A**). However, a small but significant increase in average particle size was observed ($p = 0.014$; **Fig. 5B**), suggesting minor structural changes following loading.

Zeta potential, which influences EV stability and uptake, remained in the negative range post-electroporation (−35.4 ± 1.4 mV vs. −39.0 ± 0.8 mV; $p = 0.100$), indicating that surface charge was largely retained and consistent with values expected for stable EV suspensions (**Fig. 5C**).

To assess the biodistribution kinetics and target specificity, maleimide-labelled R-28 EVs were incubated with primary rat retinal cultures for 30 minutes, 1 hour, and 2 hours. At 30 minutes and 1 hour, fluorescence was predominantly detected in DAPI$^+$/βIII-tubulin$^-$ cells, indicating preferential uptake by non-neuronal retinal cells (**Fig. 6 iA–D and 6 iiA–D**).

For comparison, EVs derived from bone marrow mesenchymal stem cells (BMSCs), previously shown to confer RGC neuroprotection (Mead & Tomarev, 2017), were also tested. BMSC-EVs were observed in both neuronal (DAPI$^+$/βIII-tubulin$^+$) and non-neuronal (DAPI$^+$/βIII-tubulin$^-$) cells at both time points (**Fig. 6 iE–H and 6 iiE–H**), suggesting broader cellular tropism.

By 2 hours post-incubation, both R-28 and BMSC-derived EVs were detected within βIII-tubulin$^+$ neurons (**Fig. 6 iiiA–H**).

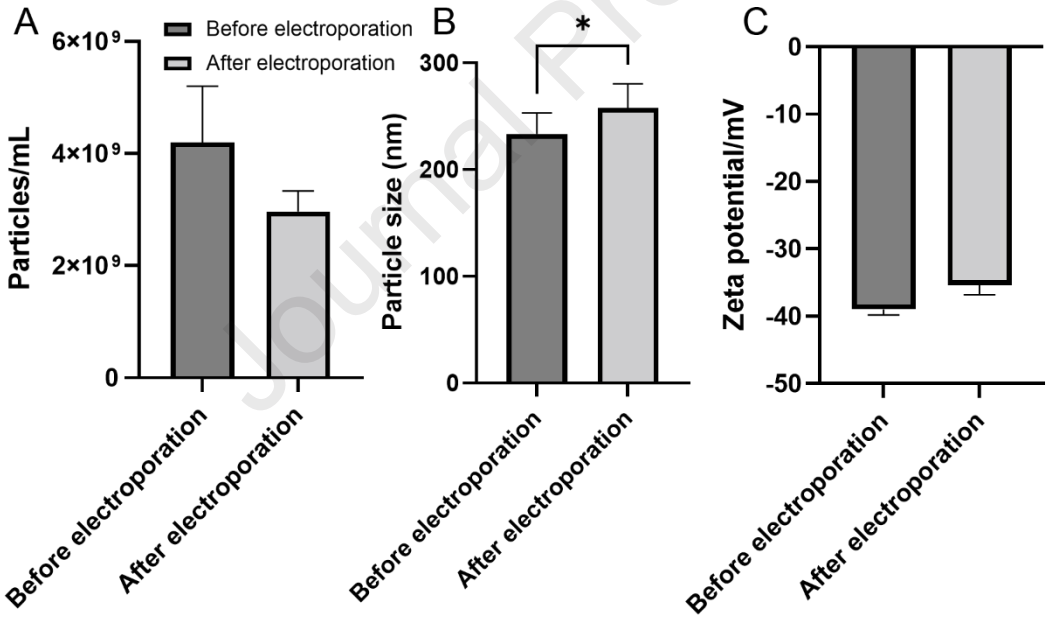

Figure 5. Impact of electroporation on EV biophysical properties. (A) EV concentration, (B) particle size, and (C) zeta potential before and after electroporation. Data shown as mean ± SEM (n = 3).

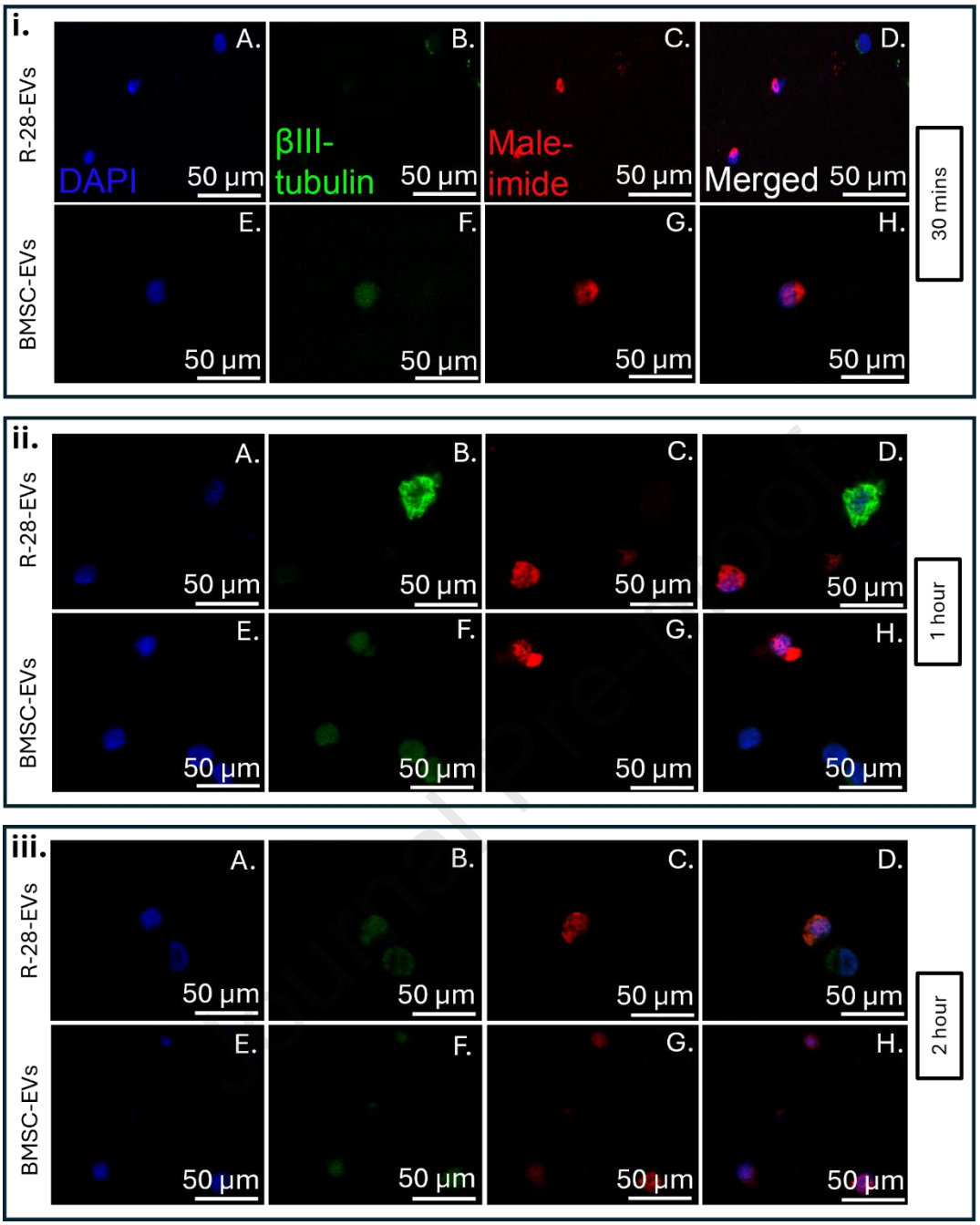

Figure 6. EV uptake dynamics and cell-type specificity in primary rat retinal cultures. R-28- and BMSC-derived EVs were labelled with maleimide (red) and incubated with primary retinal cultures for 30 min, 1 h, or 2 h. At each time point, cells were stained with DAPI (blue) and βIII-tubulin (green). Panels depict as follows: iA–D, R-28 EV uptake at 30 min; iE–H, BMSC EV uptake at 30 min; iiA–D, R-28 EV uptake at 1 h; iiE–H, BMSC EV uptake at 1 h; iiiA–D, R-28 EV uptake at 2 h; and iiiE–H, BMSC EV uptake at 2 h.

Neuroprotective efficacy of miRNA loaded EVs

To evaluate the neuroprotective effect of EVs loaded with miRNA, primary rat retinal cultures were treated and the survival assessed after 3 days (**Fig. 7A**). Treatment with miR-181a-3p (176.8 ± 14.4 RGC/well; **Fig. 7C**) or R28 EVs (148.8 ± 18.6 RGC/well) led to a significant

neuroprotective effect compared to control PBS treatment (70.5 ± 4.9 RGC/well; **Fig. 7B**), with miR-181a-3p loaded R28 EVs having the most potent effect (253 ± 16.9 RGC/well; **Fig. 7D**).

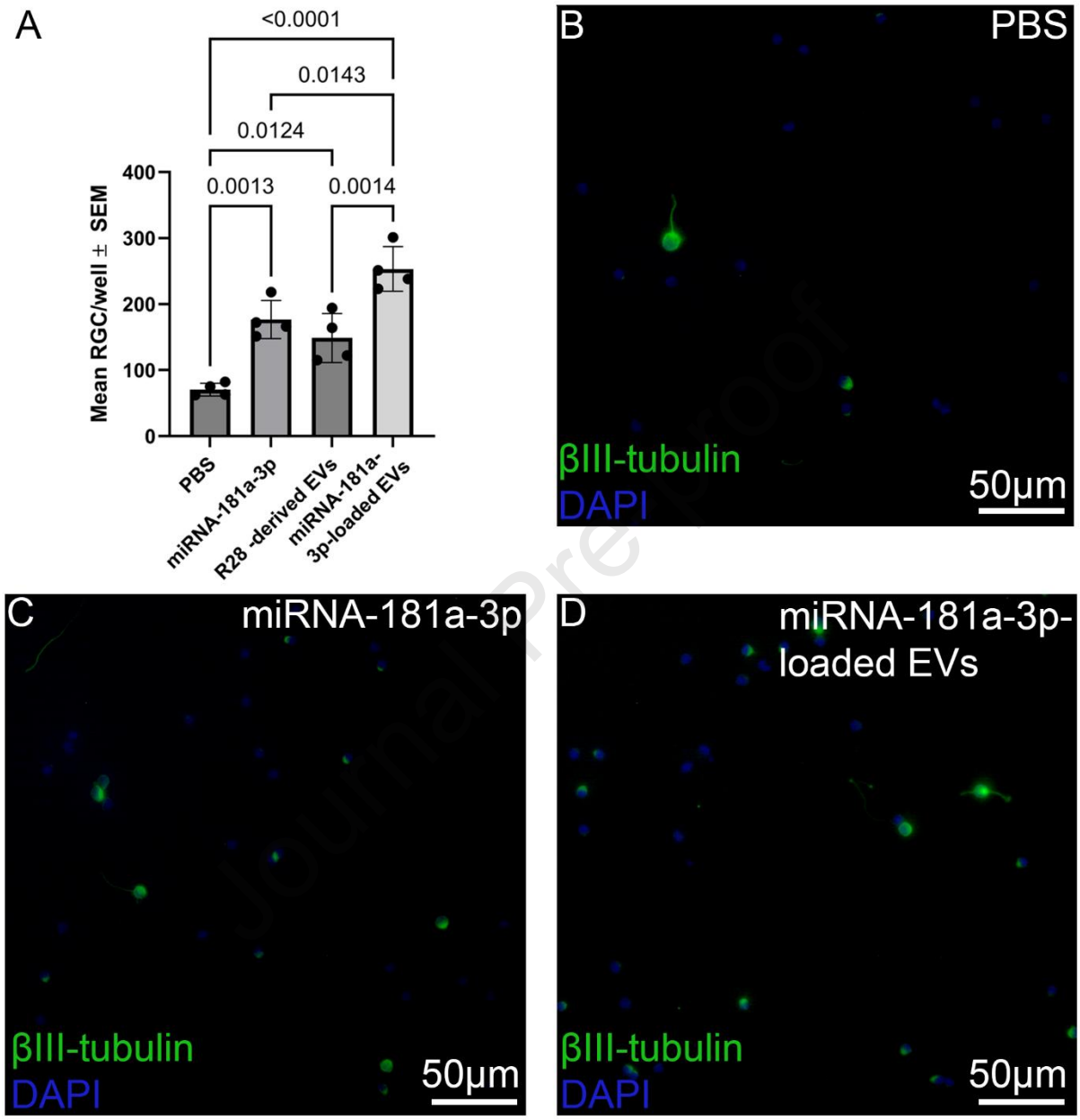

Figure 7. Neuroprotective efficacy of miRNA loaded R28 EVs on primary rat retinal cells (A)**.** Representative images of primary rat retinal cells were treated with PBS (control; B), miR 181a-3p (C), R28-derived EVs, or R28-derived EVs loaded with miR 181a-3p (D). Data shown as mean ± SEM (n = 3).

Biodistribution of miRNA loaded EVs after intravitreal injection

Fluorescence intensity of vitreal tissue as well as retina, and purified RGC was assayed 1- and 24-hours after injection of siGlo (naked or loaded into EVs; **Fig. 8**). Delivery of siRNA alone led to a modest yet significant increase in fluorescent intensity in both the retina and RGC at both 1-hour (387.3 ± 18.1 and 433 ± 24.3 AFU, respectively) and 24-hours (395.7 ± 8.1 and 383.0 ± 29.7 AFU, respectively) compared to the vitreous (194.0 ± 10.5 AFU) as well as the control (Noise) fluorescent intensity (161.3 ± 11.6 AFU). In contrast, after 1-hour, siGlo loaded EVs led to a substantial increase in the vitreous (1194.0 ± 19.8 AFU) and non-RGC retinal cells (1074.3 ± 67.3 AFU) but only a modest increase in the RGC (395.7 ± 8.1 AFU). At 24-hours, the signal was reversed, with a substantial increase in RGC (1212.3 ± 41.0 AFU), a modest increase in non-RGC retinal cells (383.0 ± 29,7 AFU), and no significant increase in the vitreous (205.0 ± 6.5 AFU).

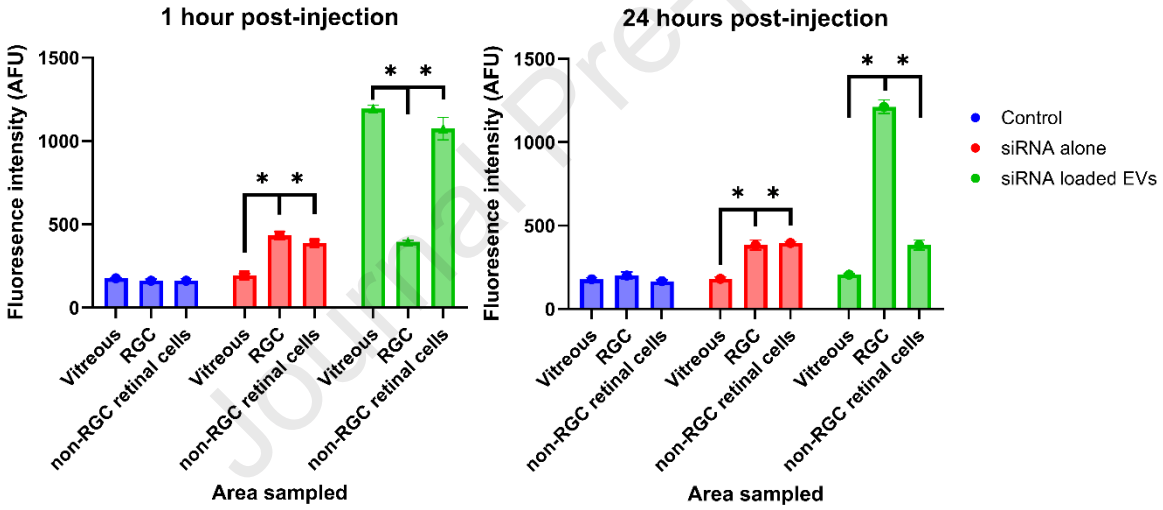

Figure 8. Biodistribution of labelled miRNA delivered *via* EVs into the vitreous body of the eye. Fluorescent siRNA (siGlo) were injected (naked or packaged in R28 EVs) into the vitreous of rats before the vitreous and retina (separated into the RGC and non-RGC) were assays for their fluorescence intensity using a fluorescence plate reader at 1- and 24-hour post-injection. Data shown as mean ± SEM (n = 3).

Discussion

There is growing interest in EVs as biologically compatible drug delivery systems, particularly for hard-to-access tissues like the retina (Zeng et al., 2023). In this study, we demonstrate that miR-181a-3p mimic confers neuroprotection to RGCs in both rodent and human-derived retinal cultures, while preserving intracellular Ca^{2+} dynamics. Moreover, when delivered via EVs, the efficiency of miRNA transfection significantly improved, though this was notably

influenced by the source of the EVs. EV origin also affected cellular targeting specificity within the retina, underscoring the importance of optimizing the EV platform for therapeutic applications.

We evaluated the RGC-protective potential of several miRNAs based on prior transcriptomic profiling in glaucomatous models (Mead et al., 2021). Among these, miR-181a-3p and miR-194-5p were the most effective at enhancing RGC survival across multiple time points. These findings align with previous reports highlighting the role of miR-181 family members in retinal homeostasis and neurodegeneration. For instance, miR-181a-3p was recently shown to promote axon regeneration in an optic nerve crush model via modulation of the p38 MAPK/ATF2 axis, further supporting its relevance as a neurotherapeutic target (Zhang et al., 2022). It has also been shown that miR-181a modulation has a protective effect on RPE and subsequently photoreceptors, in models of retinitis pigmentosa (Lopes de Costa et al., 2024). Similarly, miR-181a has been implicated in visual acuity regulation in photoreceptors (Carrella et al., 2015), hippocampal recovery post-ischemia (Griffiths et al., 2019), and mitochondrial quality control in inherited retinal disease.

Preservation of RGC function, not just survival, is essential for clinical translation. Our calcium imaging data revealed that miR-181a-3p not only improved cell survival but also enhanced neuronal Ca^{2+} signaling, indicating partial preservation of excitability. Since intracellular Ca^{2+} homeostasis is vital for synaptic activity and plasticity (Kawamoto et al., 2012), and its dysregulation is linked to neurodegenerative disease (Schank et al., 2020), this result provides functional validation of miR-181a-3p's therapeutic potential.

Pathway analysis implicated miR-181a-3p in the p38/MAPK, oxidative stress, and apoptotic signaling networks. Although p38 MAPK has a dual role in survival and degeneration (Kikuchi et al., 2000; Zarubin & Han, 2005), our qPCR validation suggested a trend toward increased MAPK14 expression, pointing to a possible stress-response modulation rather than direct toxicity.

Because commercial transfection reagents are cytotoxic to neurons (Inglut et al., 2020), we adopted EV-based delivery. Electroporation was used to load miRNAs into EVs efficiently while avoiding the toxicity associated with cationic lipid nanoparticles (Busatto et al., 2021). Both fluorescence imaging and qPCR confirmed successful EV loading and delivery of miR-181a-3p. While electroporation has been associated with siRNA aggregation (Kooijmans et al., 2013), it remains widely used for RNA loading and has shown consistent delivery efficiency (Pomatto et al., 2019; Han et al., 2024). Our findings support this, and further suggest that EV lipid structure facilitates endocytic uptake (Zhan et al., 2021; Ghadami & Dellinger, 2023).

We also examined the biophysical impact of electroporation on EVs. Although EV concentration slightly decreased and average particle size increased, these changes were modest and likely due to membrane remodeling or EV aggregation, which has been shown previously (Johnsen et al., 2016). Zeta potential remained below −30 mV, indicating preserved colloidal stability, a key factor in intravitreal delivery across the inner limiting membrane (Tavakoli et al., 2021; Durmaz et al., 2024). An alternative reason for this observation is that electroporation preferentially destroyed smaller EVs, lowering their concentration but increasing the remaining EVs average size.

We investigated EV biodistribution within retinal cultures using fluorescent maleimide labeling. R-28-derived EVs initially targeted βIII-tubulin$^-$ (non-neuronal) cells, while BMSC-derived EVs localized to both neuronal and non-neuronal targets. Our data suggest that R-28 EVs may require extended incubation to reach neurons, as confirmed by RGC targeting at later time points. Similar time-dependent distribution patterns have been observed *in vivo*. For example, MSC-EVs were found in microglia (Iba1$^+$) and RGCs (Brn3a$^+$) at 14- and 21-days post-injection, respectively (Mathew et al., 2021). Moreover, **Kim et al. (2024)** demonstrated successful EV delivery throughout the retina within 2 hours of intravitreal injection in rabbits.

To confirm that the miRNA was still therapeutically efficacious when packaged in EVs, we treated primary rat retinal cultures with loaded vs. unloaded EVs, demonstrating that miRNA is still able to exert their effects when loaded, emphasising the potential of EV loading as a viable treatment strategy.

Finally, using a fluorescently tagged RNA cargo, we sought to understand where the EV cargo distributes after delivery into the vitreous, a common injection site for targeting retinal cells. Accounting for the fluorescent noise, EVs were three times more effective at delivering a set quantity of RNA *in vivo*. EVs demonstrated greater retention in the vitreous, and an extended delay in their delivery to RGC as opposed to other retinal cells, corroborating our *in vitro* data.

The present study is not without limitations. The primary limitation lies in its *in vitro* design, which cannot fully capture the systemic and cellular complexity of *in vivo* models. While it was beyond the scope of this work to evaluate therapeutic delivery in an experimental glaucoma model, it remains possible that the degree of neuroprotection observed in rodent and human RGC cultures may not be fully recapitulated *in vivo*. Additionally, our investigation was focused specifically on miR-181a-3p; future studies should explore whether the efficiency of EV loading and delivery varies with different miRNA species or cargo types. Such comparative analyses would provide valuable insight into the generalizability and translational potential of this EV-based therapeutic platform. Finally, our observations regarding the differential uptake of EVs into different retinal cells was largely qualitative (**Fig. 6**). We were restricted to immunocytochemistry as we wanted to confirm EV uptake into the cell and limited by sample size and number of retinal cells per well. Further study using human retinal organoids would

be ideal to determine uptake selectivity in a more relevant system, as opposed to degenerating rodent retina.

The present study is not without limitations. The primary limitation lies in its *in vitro* design, which cannot fully capture the systemic and cellular complexity of *in vivo* models. While it was beyond the scope of this work to evaluate therapeutic delivery in an experimental glaucoma model, it remains possible that the degree of neuroprotection observed in rodent and human RGC cultures may not be fully recapitulated *in vivo*. Additionally, our investigation focused specifically on miR-181a-3p; future studies should explore whether the efficiency of EV loading, delivery, and therapeutic efficacy varies across different miRNA species or molecular cargos. Such comparative analyses would provide valuable insight into the generalizability and translational potential of this EV-based delivery platform. Finally, our observations regarding differential EV uptake across retinal cell types were primarily qualitative (**Fig. 6**). Immunocytochemistry was used to confirm EV internalization and subcellular localization, but quantitative assessment was limited by sample size and the number of retinal cells per well. Future studies using three-dimensional human retinal organoids or *in vivo* imaging approaches would provide a more comprehensive understanding of EV tropism and uptake kinetics within the retinal environment.

In conclusion, EVs are a more effective measure of delivering therapeutic RNA molecules to the retina, with miR-181-3p being particularly effective at protecting RGC. Loading RNA into EVs can be achieved with electroporation, and their delivery efficiency and targeting to specific retinal cells depend upon the type of EV used.

References

Alvarez-Erviti, L., Seow, Y., Yin, H., Betts, C., Lakhal, S., & Wood, M. J. A. (2011). Delivery of siRNA to the mouse brain by systemic injection of targeted exosomes. *Nature Biotechnology*, *29*(4), 341–345. https://doi.org/10.1038/NBT.1807

Brandt, S. K., Weatherly, M. E., Ware, L., Linn, D. M., & Linn, C. L. (2011). Calcium preconditioning triggers neuroprotection in retinal ganglion cells. *Neuroscience*, *172*, 387. https://doi.org/10.1016/J.NEUROSCIENCE.2010.10.071

Durmaz, E., Kutnyanszky, M., & Mead, B. (2023). Isolation and Culture of Primary Retinal Ganglion Cells from Rodent Retina. *Methods in Molecular Biology*, *2708*, 1–10. https://doi.org/10.1007/978-1-0716-3409-7_1/TABLES/2

Ghadami, S., & Dellinger, K. (2023). The lipid composition of extracellular vesicles: applications in diagnostics and therapeutic delivery. *Frontiers in Molecular Biosciences*, *10*, 1198044. https://doi.org/10.3389/FMOLB.2023.1198044/BIBTEX

Han, G., Kim, H., Jang, H., Kim, E. S., Kim, S. H., & Yang, Y. (2024). Oral TNF-α siRNA delivery via milk-derived exosomes for effective treatment of inflammatory bowel disease. *Bioactive Materials*, *34*, 138–149. https://doi.org/10.1016/J.BIOACTMAT.2023.12.010

Ilahibaks, N. F., Roefs, M. T., D Brans, M. A., Snijders Blok, C., A de Jager, S. C., Schiffelers, R. M., Vader, P., Lei, Z., G Sluijter, J. P., & Joost Sluijter, C. P. (2023). Extracellular vesicle-mediated protein delivery to the liver. *Journal of Extracellular Biology*, *2*(9), e97. https://doi.org/10.1002/JEX2.97

Izco, M., Schleef, M., Schmeer, M., Carlos, E., Verona, G., & Alvarez-Erviti, L. (2023). Targeted Extracellular Vesicle Gene Therapy for Modulating Alpha-Synuclein Expression in Gut and Spinal Cord. *Pharmaceutics 2023, Vol. 15, Page 1230*, *15*(4), 1230. https://doi.org/10.3390/PHARMACEUTICS15041230

Johnsen, K. B., Gudbergsson, J. M., Skov, M. N., Christiansen, G., Gurevich, L., Moos, T., & Duroux, M. (2016). Evaluation of electroporation-induced adverse effects on adipose-derived stem cell exosomes. *Cytotechnology*, *68*(5), 2125–2138. https://doi.org/10.1007/S10616-016-9952-7/FIGURES/6

Kawamoto, E. M., Vivar, C., & Camandola, S. (2012). Physiology and pathology of calcium signaling in the brain. *Frontiers in Pharmacology*, *3 APR*, 22359. https://doi.org/10.3389/FPHAR.2012.00061/BIBTEX

Kikuchi, M., Tenneti, L., & Lipton, S. A. (2000). Role of p38 Mitogen-Activated Protein Kinase in Axotomy-Induced Apoptosis of Rat Retinal Ganglion Cells. *The Journal of Neuroscience*, *20*(13), 5037. https://doi.org/10.1523/JNEUROSCI.20-13-05037.2000

Kim, M., Kim, J. Y., Rhim, W.-K., Cimaglia, G., Want, A., Morgan, J. E., Williams, P. A., Park, C. G., Han, D. K., & Rho, S. (2024). Extracellular vesicle encapsulated nicotinamide delivered via a trans-scleral route provides retinal ganglion cell neuroprotection. *Acta Neuropathologica Communications*, *12*(1), 65. https://doi.org/10.1186/S40478-024-01777-0

Kooijmans, S. A. A., Stremersch, S., Braeckmans, K., De Smedt, S. C., Hendrix, A., Wood, M. J. A., Schiffelers, R. M., Raemdonck, K., & Vader, P. (2013). Electroporation-induced siRNA precipitation obscures the efficiency of siRNA loading into extracellular vesicles. *Journal of Controlled Release*, *172*(1), 229–238. https://doi.org/10.1016/J.JCONREL.2013.08.014

Lu, T., Lin, Z., Ren, J., Yao, P., Wang, X., Wang, Z., & Zhang, Q. (2016). The Non-Specific Binding of Fluorescent-Labeled MiRNAs on Cell Surface by Hydrophobic Interaction. *PLoS ONE*, *11*(3). https://doi.org/10.1371/JOURNAL.PONE.0149751

Mathew, B., Torres, L. A., Gamboa Acha, L., Tran, S., Liu, A., Patel, R., Chennakesavalu, M., Aneesh, A., Huang, C.-C., Feinstein, D. L., Mehraeen, S., Ravindran, S., & Roth, S. (2021). *Uptake and Distribution of Administered Bone Marrow Mesenchymal Stem Cell Extracellular Vesicles in Retina*. https://doi.org/10.3390/cells10040730

McKinney, A. A., Petrova, R., & Panagiotakos, G. (2022). Calcium and activity-dependent signaling in the developing cerebral cortex. *Development (Cambridge)*, *149*(17). https://doi.org/10.1242/DEV.198853/276624

Mead, B., Kerr, A., Nakaya, N., & Tomarev, S. I. (2021). miRNA Changes in Retinal Ganglion Cells after Optic Nerve Crush and Glaucomatous Damage. *Cells*, *10*(7). https://doi.org/10.3390/CELLS10071564

Mead, B., & Tomarev, S. (2017). Bone marrow-derived mesenchymal stem cells-derived exosomes promote survival of retinal ganglion cells through mirna-dependent mechanisms. *Stem Cells Translational Medicine*, *6*(4), 1273–1285. https://doi.org/10.1002/sctm.16-0428

Mead, B., & Tomarev, S. (2020). Extracellular vesicle therapy for retinal diseases. *Progress in Retinal and Eye Research*, *79*. https://doi.org/10.1016/J.PRETEYERES.2020.100849

Phong, M. S., Horn, R. D. Van, Li, S., Tucker-Kellogg, G., Surana, U., & Ye, X. S. (2010). p38 Mitogen-Activated Protein Kinase Promotes Cell Survival in Response to DNA Damage but Is Not Required for the G2 DNA Damage Checkpoint in Human Cancer Cells. *Molecular and Cellular Biology*, *30*(15), 3816. https://doi.org/10.1128/MCB.00949-09

Pomatto, M. A. C., Bussolati, B., D'Antico, S., Ghiotto, S., Tetta, C., Brizzi, M. F., & Camussi, G. (2019). Improved Loading of Plasma-Derived Extracellular Vesicles to Encapsulate Antitumor miRNAs. *Molecular Therapy Methods and Clinical Development*, *13*, 133–144. https://doi.org/10.1016/j.omtm.2019.01.001

Schrank S, Barrington N, Stutzmann GE. Calcium-Handling Defects and Neurodegenerative Disease. Cold Spring Harb Perspect Biol. 2020 Jul 1;12(7):a035212. doi: 10.1101/cshperspect.a035212. PMID: 31427373; PMCID: PMC7328457.

Shimizu, A., Sawada, K., Kobayashi, M., Oi, Y., Oride, T., Kinose, Y., Kodama, M., Hashimoto, K., & Kimura, T. (2024). Patient-Derived Exosomes as siRNA Carriers in Ovarian Cancer Treatment. *Cancers*, *16*(8), 1482. https://doi.org/10.3390/CANCERS16081482/S1

Suggate EL, Ahmed Z, Read ML, et al. Optimisation of siRNA-mediated RhoA silencing in neuronal cultures. *Mol Cell Neurosci*. 2009;40:451–462.

Yang, J., Zhang, X., Chen, X., Wang, L., & Yang, G. (2017). Exosome Mediated Delivery of miR-124 Promotes Neurogenesis after Ischemia. *Molecular Therapy - Nucleic Acids*, *7*, 278–287. https://doi.org/10.1016/J.OMTN.2017.04.010

Zarubin, T., & Han, J. (2005). Activation and signaling of the p38 MAP kinase pathway. *Cell Research 2005 15:1*, *15*(1), 11–18. https://doi.org/10.1038/sj.cr.7290257

Zeng, H., Guo, S., Ren, X., Wu, Z., Liu, S., & Yao, X. (2023). Current Strategies for Exosome Cargo Loading and Targeting Delivery. *Cells*, *12*(10). https://doi.org/10.3390/CELLS12101416

Zhan, Q., Yi, K., Li, X., Cui, X., Yang, E., Chen, N., Yuan, X., Zhao, J., Hou, X., & Kang, C. (2021). Phosphatidylcholine-Engineered Exosomes for Enhanced Tumor Cell Uptake and Intracellular Antitumor Drug Delivery. *Macromolecular Bioscience*, *21*(8), 2100042. https://doi.org/10.1002/MABI.202100042

- miR-181a-3p identified as a lead neuroprotective microRNA for retinal ganglion cells.
- Electroporation effectively load miRNA into EVs
- R-28 retinal cell–derived extracellular vesicles efficiently delivered miR-181a-3p.
- EV-mediated delivery enhanced retinal ganglion cell survival and calcium signaling.
- Intravitreal EV-miRNA delivery achieved selective retinal uptake

I certify that all co-authors have read and agreed to the contents of the manuscript and there is no financial interest to report. We certify that the submission is original work and is not under review at any other journal.